Simultaneous Laser-Induced Fluorescence of Nitric Oxide and Atomic Oxygen in the Hypersonic Materials Environment Test System Arcjet Facility

Craig Johansen[1,*], Daniel Lincoln[1], Brett Bathel[2], Jennifer Inman[2], Paul Danehy[2]

1: Department of Mechanical and Manufacturing Engineering, University of Calgary, Calgary, Canada
2: NASA Langley Research Center, Hampton, United States
* correspondent author: johansen@ucalgary.ca

Abstract Simultaneous nitric oxide (NO) and atomic oxygen (O) laser induced fluorescence (LIF) experiments were performed in the Hypersonic Materials Environmental Test System (HYMETS) facility at the NASA Langley Research Center. The data serves as an experimental database for validation for chemical and thermal nonequilibrium models used in hypersonic flows. Measurements were taken over a wide range of stagnation enthalpies (6.7 – 18.5 MJ/kg) using an Earth atmosphere simulant with a composition of 75% N2, 20% O2, and 5% Ar (by volume). These are the first simultaneous measurements of NO and O LIF to be reported in literature for the HYMETS facility. The maximum O LIF mean signal intensity was observed at a stagnation enthalpy of approximately 12 MJ/kg while the maximum NO LIF mean signal intensity was observed at a stagnation enthalpy of 6.7 MJ/kg. Experimental results were compared to simple fluorescence model that assumes equilibrium conditions in the plenum and frozen chemistry in the isentropic nozzle expansion (Mach 5). The equilibrium calculations were performed using CANTERA v2.1.1 with 16 species. The fluorescence model captured the correlation in mean O and NO LIF signal intensities over the entire range of stagnation enthalpies tested. Very weak correlations between single-shot O and NO LIF intensities were observed in the experiments at all of the stagnation enthalpy conditions.

1. Introduction

Arcjet facilities can produce high-enthalpy, hypersonic, and non-equilibrium flows, and are typically used for the thermostructural development of materials for re-entry vehicles. Unique to these facilities is the ability to produce thermal environments corresponding to flight Mach numbers of 8 to 20 over long run times.[1] Since the 1960s, spectroscopic and electrostatic (e.g. Langmuir probe) techniques have been used in arcjet facilities to extract quantitative data from the flow.[2] Although impulse facilities such as shock and expansion tubes and tunnels can produce flows over a large Mach number range and at high enthalpy, they operate on very short time-scales, inhibiting the use of many types of diagnostics. With longer run-times associated with arcjet facilities, laser diagnostics that require longer time-scales become more feasible. For example, Doppler-shift planar laser-induced fluorescence (PLIF) velocimetry can require spectral scanning of a high-energy laser source, which can take on the order of minutes to complete when using a typical dye-pumped pulsed laser operating at a frequency of 10 Hz. In an impulse facility, only a single measurement can be obtained during a run when using 10 Hz equipment. Therefore, a large number of runs become necessary to resolve a single transition. For example, Hruschka et al., (2010) performed two-component Doppler-shift nitric oxide (NO) PLIF velocimetry in the T-ADFA free piston shock tunnel running at a stagnation enthalpy of 3.8 MJ/kg and a freestream Mach number of 10.[3] In these tests, 29 tunnel runs were required to resolve the $^RR_{22}(14)$ transition used to extract the radial velocity distribution in the wake of a capsule model. In contrast, Inman et al., (2013) obtained Doppler-shift NO PLIF velocimetry measurements in a single run of the Hypersonic Materials Environment Test System (HYMETS) arcjet facility.[4][**Error! Reference source not found.**] Over a duration of 45 seconds, the $^QQ_{11}(13)$ NO transition was resolved using a scanning laser to extract the radial velocity distribution ahead of a heat-shield model in a Mach 5 flow with a stagnation enthalpy of 6.5 MJ/kg. Often, the interpretation of tunnel data first requires facility characterization. A large part of the work reported by Inman et al. (2013) in the HYMETS facility was the qualitative characterization of NO concentrations in the freestream at various stagnation enthalpies.[4] Measuring the effect of tunnel operating conditions on additional species concentrations will further aid in the validation effort for nonequilibrium

models. In particular, simultaneous concentrations of NO and atomic oxygen (O) would be useful in the study of thermal and chemical nonequilibrium associated with the rapid expansion high-temperature air in these facilities.

There have been some works reported in the literature where simultaneous LIF signals from multiple species have been acquired in a single experiment. Although not in a hypersonic flow facility, some of the first demonstrations of simultaneous NO and O LIF were performed in laboratory flames. Westblom and Aldén (1989) showed simultaneous spectral scans of NO, O, and OH in a H_2/N_2O flame.[5] Similarly, Wysong et al., (1989) performed simultaneous O, O_2, and NO in a lean H_2/O_2 flame.[6] In these works, the overlap in the excitation spectra of these species made the simultaneous measurements possible. LIF measurements of multiple species have also been performed in hypersonic flow facilities. Fletcher (1999) gives an overview of nonintrusive diagnostic strategies for arcjet stream characterization, where he highlights a few experiments where LIF from multiple species was obtained, though not simultaneously.[7] Vecchio et al., (2000) performed LIF measurements of NO and O in the L2K arcjet facility of DLR.[8] Although not simultaneous, they reported rotational temperatures for both NO and O across the bow shock ahead of a blunt model for stagnation enthalpies of 7.3 and 8.85 MJ/kg and free stream Mach numbers of roughly 5.7 to 8.4. Mirzuno et al., (2007) performed simultaneous LIF measurements of NO and O in the JAXA arcjet facility.[9] They spectrally scanned their laser source over multiple NO and O transitions and recorded the excitation spectra on separate ICCD cameras. The effect of the stagnation enthalpy on NO and O LIF values was described qualitatively. However, they did not discuss any correlations between single shot NO and O values. To the authors' knowledge, there is no literature reporting simultaneous NO and O LIF measurements in a hypersonic flow facility over a wide range of tunnel stagnation enthalpies. In addition, previous works that have performed simultaneous NO and O LIF measurements have not studied the potential correlation between instantaneous NO and O LIF fluctuations. In this work, simultaneous NO and O-atom LIF measurements are obtained in the freestream of the HYMETS facility for a wide range of stagnation enthalpies (6.7–18.5 MJ/kg). These are the first simultaneous measurements of NO and O LIF to be reported in the literature for the HYMETS facility. The correlation of single shot fluctuations of NO and O-atom LIF are discussed. The experimental results are compared to equilibrium calculations.

2. Facility and Experimental Setup

The HYMETS facility is located at the NASA Langley Research Center. A 400 kW power supply is used to run a segmented-constrictor direct-current electric arc heater, which serves as the arc plasma generator. Test gasses are injected tangentially into the bore to produce a vortex flow, which spin-stabilizes the electric arc of the plasma generator. The heated mixture is then accelerated through a convergent-divergent 8-degree half-angle Mach 5 conical nozzle with a 12.7-mm diameter throat. To increase the footprint of the arc and thus protect the electrodes from rapid oxidation, argon (Ar) is injected near the anode. After passing through the test section, the flow exhausts into a 0.6-m diameter by 0.9-m long vacuum test chamber. A high capacity pumping system is used to evacuate the stagnated flow from the facility after being cooled. Depending on the tunnel conditions, the facility can be operated by a single technician, continuously, and for several hours.

Figure 1 (left) shows a top-view schematic of the HYMETS facility with forward (blue) and return (red) laser beams needed to perform the simultaneous NO and O LIF excitation experiment. The beams originated from a pulsed Spectra Physics Pro-230 Nd:YAG laser that was used to generate 1064 nm light.
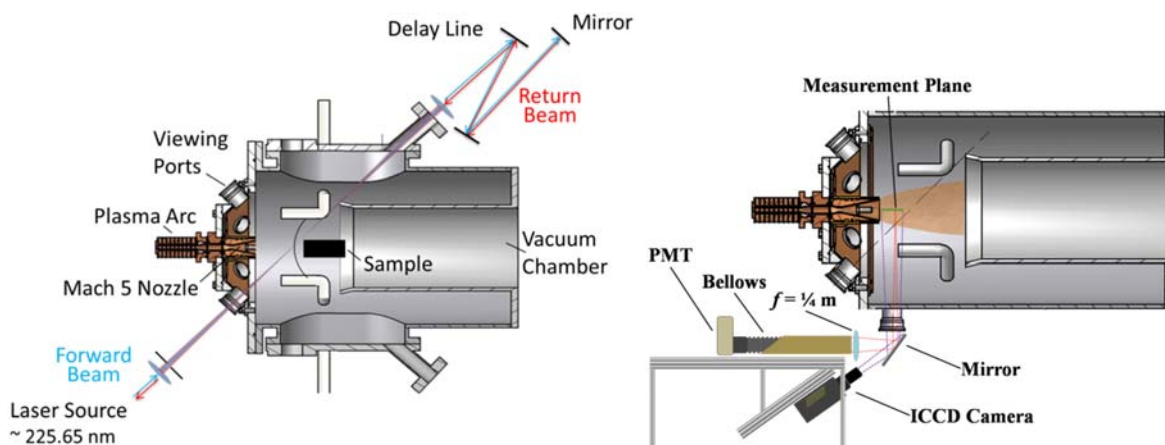
Fig. 1 Top-view (left) and side-view (right) schematics of HYMETS facility with NO and O-atom LIF setup. Adapted from Refs. 4 and 10.

This 1064 nm output was then frequency doubled to produce 532 nm, which subsequently pumped a Sirah Cobra Stretch dye laser to achieve a ~623 nm output beam. The 1064 nm light was also frequency tripled to produce 355 nm light. The 623 nm and 355 nm light were then sum frequency mixed in a Sirah Frequency Conversion Unit (FCU) to produce a 226 nm beam. This 226 nm beam had a spectral width of approximately 0.07 cm^{-1}. The duration of the pulse at 226 nm was approximately 10 ns at a 10 Hz repetition rate. This light was used to excite the two-photon transition from the J = 0 transition of O and the overlapping $Q_1(6.5)$ + $P_{21}(6.5)$ transitions of NO. Figure 2 shows a spectral scan of the O and NO transitions.
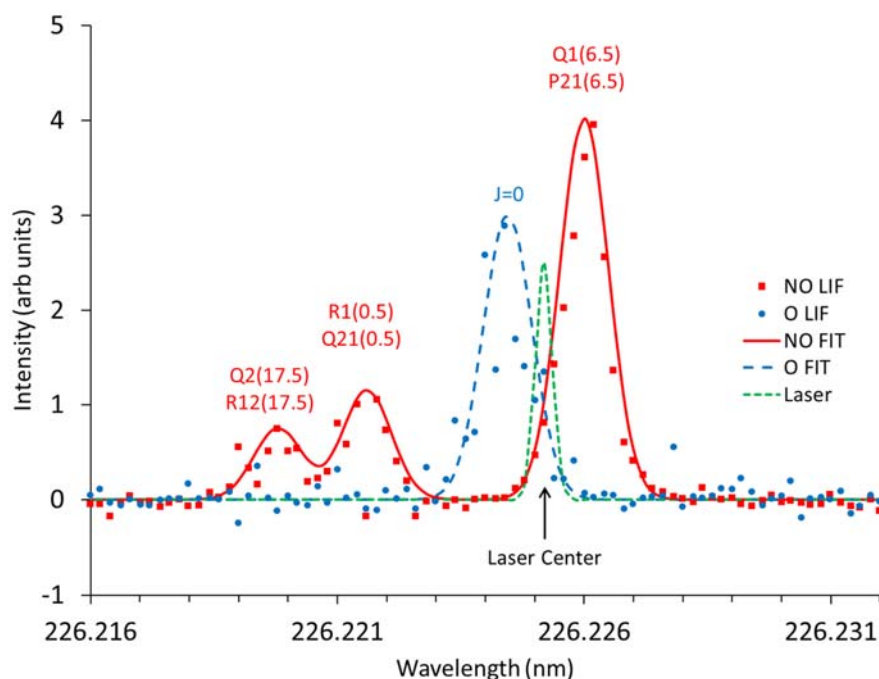

Fig. 2 Spectral scan of O and NO transitions. NO LIF from NO gas reference cell. O LIF from inside facility at test condition 9 (150 A, 425 slpm).

The 226 nm beam was then passed through a 1-m focal length spherical lens and subsequently passed through a UV-transmitting viewing port on the HYMETS facility. This beam (hereafter called the *forward* beam) passed through the test section, focusing downstream of the Mach 5 nozzle along its axis of

symmetry, and exited a rear-facing viewing port. The beam then passed through another 1-m focal length spherical lens which collimated the beam prior to entering into an optical delay line. The beam (referred to as the *return* beam) was then redirected back through the 1-m focal length spherical lens and rear-facing viewing port. The beam again passed through the test section, again focusing downstream of the nozzle along its axis of symmetry. Both the forward and return beams were aligned such that they were collinear. Figure 3 shows a schematic of the paths of the forward (blue) and return (red) laser beams inside the test section. The use of the delay line allowed for Doppler-based velocimetry measurements in subsequent tests, the results of which are reported elsewhere.[11] It also removed the need for an independent wavelength calibration for the laser. The temporal separation (approximately 10 ns) of the forward and return beams at the point of focus was much shorter than the flow time scale. As such, the flow is effectively stationary between the two pulses.
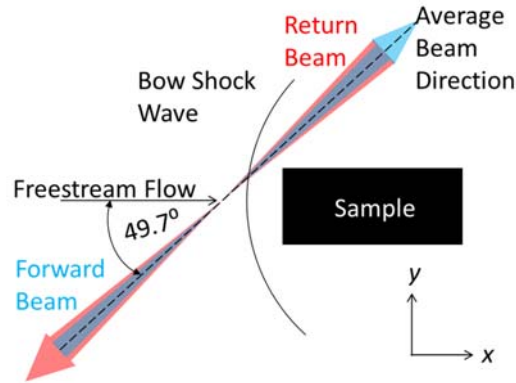

Fig. 3 Zoomed in schematic of sample showing laser beam direction relative to sample and freestream flow. Adapted from Ref. 10. In the present work, the sample was not injected into the flow and measurements were made in the freestream.

Figure 1 (right) shows a side-view schematic of the HYMETS facility and NO/O-atom imaging system. A Hamamatsu R758-10 photomultiplier tube (PMT) was used to collect the infrared O-atom LIF emission through a viewing port at the bottom of the facility. An 850 nm notch filter was placed at the entrance of the PMT to pass the infrared LIF O-atom emission. A silvered mirror was mounted below this viewing port to direct LIF emission towards the imaging system. A bellows in combination with a beam tube was used to prevent ambient light, which would otherwise reduce measurement sensitivity, from entering the PMT. A ¼-m focal length spherical lens was placed at the exit of the bellows so that the PMT only imaged a single point in the measurement plane. The NO LIF signal along the laser paths was captured in a series of images using a Princeton Instruments PIMAX-2 intensified CCD camera with a 512 x 512 pixel array. A UV filter (Layertec GmbH: <1% transmission at 226 nm; >80% from 235 nm – 280 nm) was used to block the laser wavelength but pass the NO LIF emission to the camera's imaging sensor. This camera was mounted below the test section and viewed the measurement region by looking at a silvered mirror mounted below the bottom viewing port.

3. Results

Table 1 shows a list of the test conditions with the corresponding bulk enthalpy, arc current, mass flow rate, and arc pressure. The bulk enthalpy is determined by monitoring the water temperature at the inlet and outlet of the arc column and monitoring the input power to the arc (product of current and voltage).[12]**Error! Reference source not found.** In the tests, a mixture of 75% N_2, 20% O_2, and 5% Ar was used to approximate the composition of Earth's atmosphere. Note that standard dry air has a composition of roughly 78% N_2, 21% O_2, and 1% Ar. The additional 4% Ar in the test gas is used to reduce degradation of the anode. Equilibrium calculations were performed using the software CANTERA v2.1.1 with the high temperature thermal library, airNASA9.cti.[13] The species included in the calculation were O, O_2, Ar, N, N_2, NO, O^+, O^-, O_2^+, O_2^-, N^+, N^-, N_2^+, NO^+, Ar^+, and e^-.

Test	Bulk Enthalpy (MJ/kg)	Arc Current (Amps)	Mass Flow (slpm)	Arc Pressure (kPa)
1	6.7	100	403	110.5
2	8.3	125	404	118.5
3	9.9	150	404	125.7
4	11.3	174	404	133.0
5	11.7	150	304	100.8
6	13.1	150	254	84.8
7	15.8	151	179	63.5
8	18.5	150	129	46.0

Table 1 Test conditions

To assess the accuracy of the predictions, equilibrium calculations of dry air were performed over a temperature range of 1000 K < T < 6000 K with CANTERA v2.1.1 (using both airNASA9.cti and nasa_gas.cti libraries), the Colorado State University Chemical Equilibrium Calculator (using STANJAN), and the NASA CEA Solver.[14-16] Excellent agreement between each of the solvers was observed for the predicted composition over the entire temperature range. The maximum discrepancy between predicted O mole fractions was 0.9% and occurred at 2000 K. The maximum discrepancy between predicted NO mole fractions was 0.76% and occurred at 6000 K. However, there were large discrepancies between the solver predictions and the published data of Henderson and Menart (2008) and Hilsenrath and Klein (1965).[17,18] For O mole fractions, the largest discrepancy was 69% and occurred at 3000 K. For NO, the largest discrepancy was 446% and occurred at 6000 K. The authors are unclear why there is such a good agreement between various equilibrium solvers (using high temperature thermal libraries) but such poor agreement between the solver predictions and the published data of Henderson and Menart (2008) and Hilsenrath and Klein (1965). Note that an equilibrium calculation based on a procedure and equilibrium constants published by Cengel and Boles (2010)[19] showed good agreement with the equilibrium solver predictions. Therefore, CANTERA was used to calculate the equilibrium composition for each of the experimental test conditions in the HYMETS facility.

For the equilibrium calculations, the stagnation pressure and stagnation temperature were based on the pressure measurements near the plasma arc and inferred from bulk enthalpy measurements, respectively (Table 1). Specifically, the stagnation temperature was determined through interpolation of the equilibrium results that were performed over a small temperature range at each pressure condition. Figure 4 shows the stagnation pressure and stagnation temperature corresponding to each test condition. The pressure ranged from 46 to 133 kPa while the stagnation temperature ranged from roughly 3800 K to 6200 K.
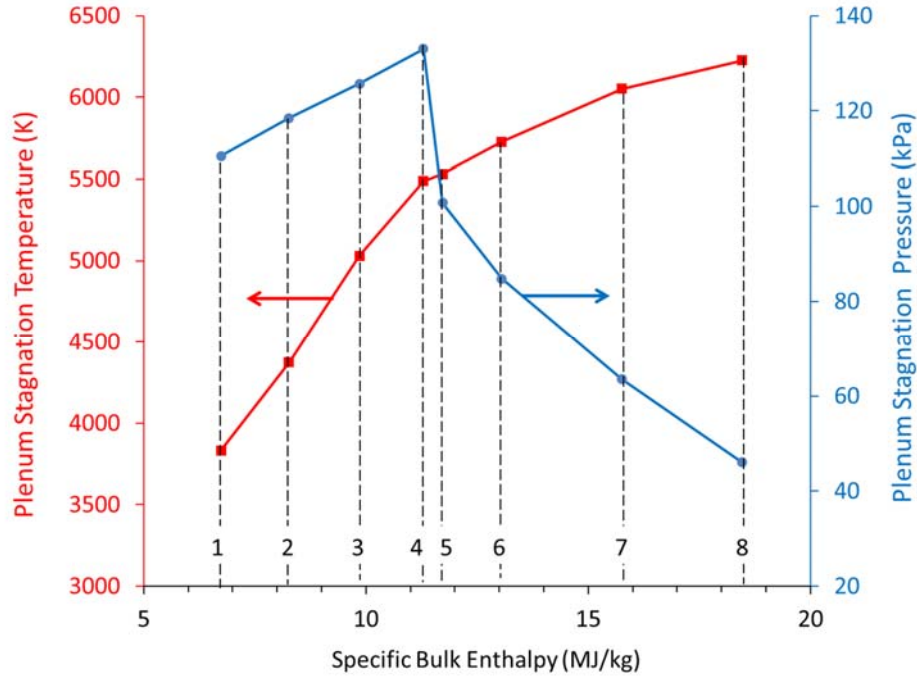
Fig. 4 Calculated equilibrium stagnation temperature and measured arc pressure as a function of specific bulk enthalpy. Test conditions indicated at bottom of graph. Arrows indicate the relevant dependent axis for each data set.

As the flow expanded through the nozzle into the test section, overall concentrations levels were expected to decrease. Figure 5 shows the calculated freestream pressure and temperature corresponding to each test condition. The calculation assumed that the flow was in thermal and chemical equilibrium in the plasma arc plenum and was chemically frozen as it expanded isentropically through the Mach 5 nozzle into the test chamber. Mixture specific heats were calculated from each equilibrium composition, but were also assumed frozen during the expansion. Because the flow in the arc plenum is subsonic with a relatively long residence time, it is a common practice to assume that the gas mixture achieves thermal and chemical equilibrium.[8] However, experiments in the NASA Ames Aerodynamic Heating Facility (AHF) Arcjet suggest that chemistry becomes frozen within the nozzle and chemical composition can change initially after leaving the plenum.[7] Therefore, an error in the predicted chemical composition of the free-stream is expected, the magnitude of which is unknown.
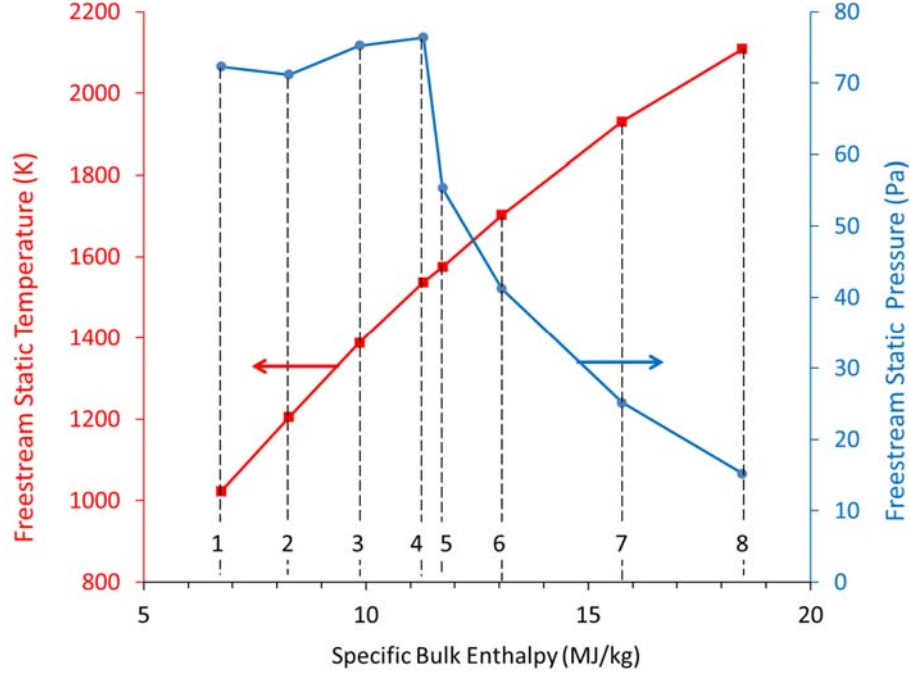
Fig. 5 Calculated freestream temperature and pressure as a function of specific bulk enthalpy. Test conditions indicated at bottom of graph. Arrows indicate the relevant dependent axis for each data set.

A LIF signal (S_{LIF}) from a probed species depends on many factors including the mole fraction (χ_s), total number density of all species present (N_T), Boltzmann fraction (f_B), Einstein coefficient for stimulated absorption (B_{12}), incident laser irrandiance (I), overlap integral (G), fluorescence yield (Φ), period of the detection (t_{det}), probed volume (V), and factors related to the detection optics ($\frac{\Omega}{4\pi}\eta$):[20]

$$S_{LIF} = \chi_s f_B N_T B_{12} I G \Phi t_{det} V \frac{\Omega}{4\pi} \eta \tag{1}$$

Note that η and Ω are the detection efficiency and the solid angle subtended by the detector, respectively. Since the same optical path was used at each test condition, a comparison of relative LIF signals is mainly affected by the species concentration ($\chi_s N_T$) and the Boltzmann fraction. Although the overlap integral and the fluorescence yield might also be affected by changing run conditions, they were not analyzed in this work. However, an analysis of the fluorescence lifetime (assuming standard air with 1% NO) indicates a maximum variation of 5% in the fluorescence yield over the range of test conditions. Note that qualitative comparisons between experimental LIF signal intensities and computed concentrations of the probed species are commonly reported.[21] The Boltzmann fraction for the NO species was based on the following estimation:

$$f_B = \frac{(2J"+1)}{Z_{Total}} e^{\left(\frac{-hcB_v}{kT}J"(J"+1)\right)} \tag{2}$$

Here, J" = 6.5 is the rotational quantum number of the ground state, $k = 1.38 \times 10^{-23}$ J/K is the Boltzmann constant, $h = 6.62607 \times 10^{-23}$ J·s is Planck's constant, $c = 299792458$ m/s is the speed of light in a vacuum, and $B_v = 169.57$ m^{-1} is the rotational constant for NO.[22]**Error! Reference source not found.** In this work, the non-dimensional value of $kT/(hcB_v)$ ranged between 418 and 864. Eckbreth (1996) gives the following approximation for the total partition function (Z_{Total}) in the case of large $kT/(hcB_v)$ values:[23]

$$Z_{Total} = \frac{kT}{hcB_v} \tag{3}$$

Using the approximation for the total partition function, the Boltzmann fraction corresponding to the NO transition becomes:

$$f_B = \frac{hcB_v}{kT}(2J'' + 1)e^{\left(\frac{-hcB_v}{kT}J''(J''+1)\right)} \qquad (4)$$

The Boltzmann fraction corresponding to the excitation of the electronic ground state of O is approximated as:[24]

$$f_B = \frac{g_0}{g_0 + g_1 e^{-\Theta_1/T} + g_2 e^{-\Theta_2/T} + g_3 e^{-\Theta_3/T}} \qquad (5)$$

where the degeneracy factors are $g_0 = 5$, $g_1 = 3$, $g_2 = 1$, and $g_3 = 1$ and the characteristic temperatures of electronic excitation are $\Theta_1 = 228$ K, $\Theta_2 = 526$ K, and $\Theta_3 = 2300$ K. Note that higher order terms have been truncated in the electronic partition function (denominator in Eq. 5).

Figure 6 shows a comparison between LIF measurements (data points), calculated equilibrium concentrations in the freestream (solid curves, assuming frozen chemistry), and estimated fluorescence values in the freestream (dashed curves, including the Boltzmann distribution). The concentration of O and NO are denoted as [O] and [NO], respectively. Although the laser source and interrogation region were identical for both the O and NO LIF measurements, different collection optics were used (PMT vs. PIMAX-2 intensified CCD camera). Therefore, the LIF intensity corresponding to each species was normalized by their respective maximum values (corresponding to enthalpy condition). Similarly, the computed NO and O values were also normalized by their respective maximum values over the enthalpy range.
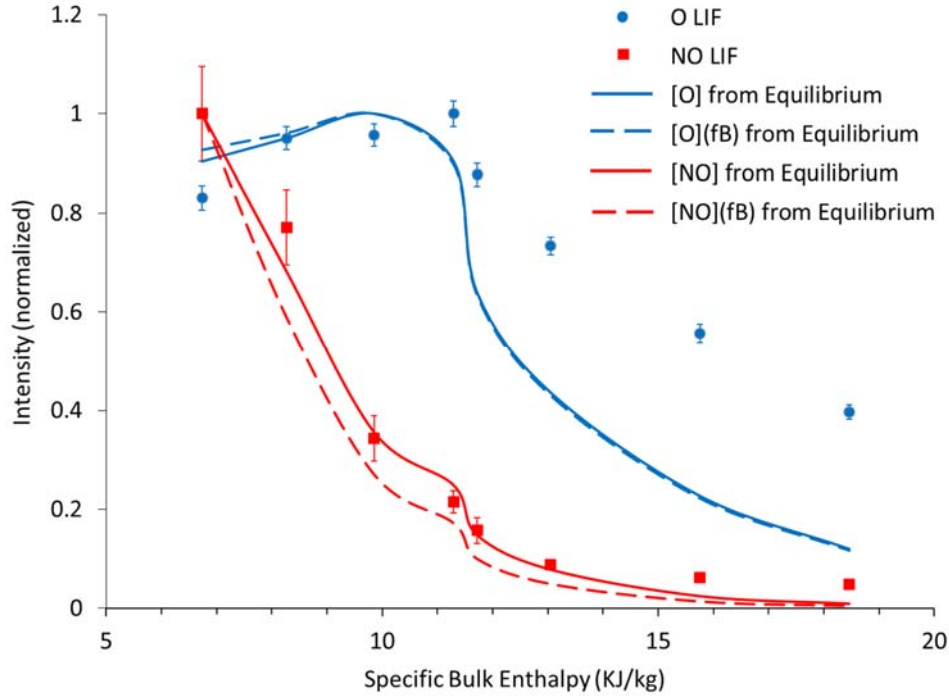

Fig. 6 Normalized intensities of O and NO fluorescence compared to equilibrium calculations. Standard error indicated by error bars.

Each experimental data point shown in Fig. 6 is an average of 120 measurements. The NO LIF and equilibrium calculation data show a trend of decreasing intensity with increasing enthalpy. This is expected since equilibrium calculations (at 1 atm) indicate that the NO mole fraction peaks near 10.3 MJ/kg ($T_{stag} = 5000$ K) and then steadily decreases as NO molecules dissociate at higher temperatures. Furthermore, the decrease in pressure and increase in temperature serves to further lower the overall gas density at the higher enthalpy conditions. The O LIF signal initially increases and peaks near an enthalpy of 10 MJ/kg ($T_{stag} = $

4800 K) and then decreases at higher enthalpies. Equilibrium calculations (1 atm) indicate that the O mole fraction peaks near 20 MJ/kg (T_{stag} = 6500 K) and slowly decreases at higher temperatures. However, as the arc pressure decreases at higher enthalpies (Fig. 4), the density of O decreases in the freestream. The combined effect is a peak in fluorescence at a stagnation enthalpy of approximately 12 MJ/kg. It was found that the inclusion of the Boltzmann fraction has a negligible effect on the computed O values and a small (adverse) effect on the computed NO values relative to the experiment.

Figure 7 shows the correlation between O and NO fluorescence at each test condition. Equilibrium calculations (including the effect of the Boltzmann distribution) are overlaid onto the graph as a solid line. It appears that the equilibrium calculations are able to capture the relationship between O and NO fluorescence signals over a wide range of tunnel conditions.
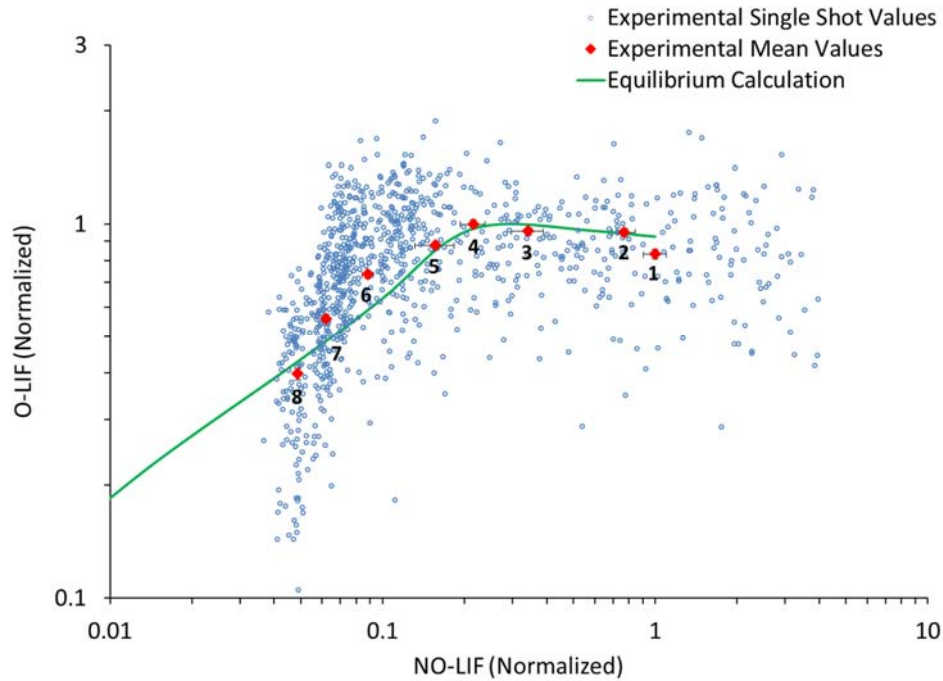

Fig. 7 Correlation between O and NO fluorescence and comparison to equilibrium calculation. Test conditions indicated as numbers in the figure.

Interestingly, only weak, if any, correlations were found between single-shot NO and O LIF values within any single test condition, as demonstrated in Fig. 8. It is possible that in chemical nonequilibrium, fluctuations of NO are not accompanied by fluctuations in O. For example, the chemical rate equation for NO depends on concentrations of O_2, N, N_2, and e[-] as well as concentrations of O.[25] Therefore it is possible that the time scales associated with concentration fluctuations are too short to observe a strong correlation of fluorescence between the species.
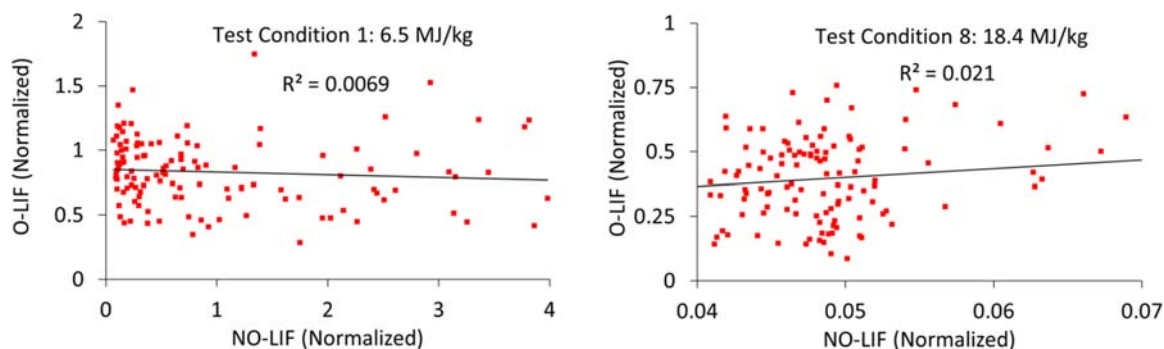
Fig. 8 Single-shot correlations between O and NO fluorescence. Lowest (left) and highest (right) enthalpy conditions are shown.

One possible error in the experiment is the potential misalignment between the NO and O probe volumes. Misalignment would have a large effect on the single-shot correlations. Multiple realignments using a small hydrogen flame and optimization of LIF signals before each test should have minimized this error. However, in a future experiment, either the same collection optic could be used for both NO and O LIF channels if making single-point measurements or two separate cameras could be used, allowing the images to be correlated and position errors quantified, if two-dimensional measurements were obtained. In contrast to its effect on single shot correlations, a small misalignment should not have a large effect on the correlations between mean NO and O LIF signals. Collisional quenching could also lead to an error in the experimental LIF signals. Analysis of the pulse shapes obtained in the experiment could be performed to correct for this error. Furthermore, computation of the overlap integral might also improve agreement between computations and experiment. Errors in the equilibrium calculations mainly stem from any inaccuracies in the underlying assumptions. These include chemical and thermal equilibrium in the plenum, frozen chemistry in the nozzle expansion, isentropic flow in the nozzle expansion, and thermal equilibrium in the nozzle expansion. A full nonequilibrium calculation of the flow at each condition could help quantify the validity of these assumptions.

4. Conclusions

Simultaneous NO and O LIF data has been reported in the HYMETS arcjet facility for the first time. Experiments show a clear relationship between tunnel stagnation enthalpy and mean concentrations of NO and O. Equilibrium calculations based on conditions near the plasma arc generator predict the trend in NO and O LIF intensities as the enthalpy conditions in the facility are varied. The correlation between mean O and NO signals is also predicted by the equilibrium calculations. There appears to be very weak, if any, correlation between single-shot O and NO fluorescence values at either test condition.

Acknowledgements

References

[1] D.M. Smith, E.J. Felderman, F.L. Shope, and J.A. Balboni, "Arc-Heated Facilities" in *Advanced Hypersonic Test Facilities*, Progress in Astronautics and Aeronautics Vol 198, pp. 279-311.

[2] C.D. Scott, "Survey of Measurements of Flow Properties in Arcjets," *Journal of Thermophysics and Heat Transfer,* Vol. 7, No. 1, pp. 9-24, 1993.

[3] R. Hruschka, S. O'Byrne, and H. Kleine, "Two-component Doppler-shift fluorescence velocimetry applied to a generic planetary entry probe model," *Exp. Fluids*, Vol. 48, pp. 1109-1120, 2010.

[4] J. Inman, B. Bathel, C. Johansen, P. Danehy, S. Jones, J. Gragg, and S. Splinter, "Nitric oxide planar laser-induced fluorescence measurements in the Hypersonic Materials Environment Test System," AIAA Journal, Vol. 51, No. 10, pp. 2365-2379, 2013.

[5] U. Westblom and M. Aldén, "Simultaneous multiple species detection in a flame using laser-induced fluorescence," Applied Optics, Vol. 28., No. 13, pp. 2592-2599, 1989.

[6] I.J. Wysong, J.B. Jeffries, and D.R. Crosley, "Laser-Induced Fluorescence of $O(3p^3P)$, O_2, and NO near 226 nm: photolytic interferences and simultaneous excitation in flames," Optics Letters, Vol. 14, No. 15, pp. 767-769, 1989.

[7] D.G. Fletcher, "Nonintrusive Diagnostic Strategies for Arcjet Stream Characterization," Defence Technical Information Center Compilation Part Notice ADP010741, RTO AVT Course, Rhode-Saint-Genese, Belgium, 1999.

[8] A. Vecchio, G. Palumbo, U. Koch, A. Gulhan, "Temperature Measurements by Laser-Induced Fluorescence Spectroscopy in Nonequilibrium High-Enthalpy Flow," *AIAA Journal of Thermophysics and Heat Transfer,* Vol. 14, No. 2, pp. 216-224, 2000.

[9] M. Mirzuno, T. Ito, K. Ishida, J. Nagai, "Laser Induced Fluorescence of Nitric Oxide and Atomic Oxygen in an Arc Heated Wind Tunnel," AIAA 2007-4405, 39th AIAA Thermophysics Conference, June 25-28, 2007.

[10] B.F. Bathel, C.T. Johansen, J.A. Inman, S.B. Jones, and P.M. Danehy, "Review of Fluorescence-Based Velocimetry Techniques to Study High-Speed Compressible Flows," 51st AIAA Aerospace Sciences Meeting, AIAA Paper 2013-0339, Grapevine, TX, January 4 – 7, 2013.

[11] B.F. Bathel, C.T. Johansen, J.A. Inman, S.B. Jones, and P.M. Danehy, "Review of Fluorescence-based Velocimetry Techniques to Study High-Speed Compressible Flows (Invited)", AIIAA Paper 2013-0339, 51st AIAA Aerospace Sciences Meeting including the new Horizons Forum and Aerospace Exposition, January 7-10, Grapevine, TX, 2013.

[12] S.C Splinter, K.S. Bey, J.G. Gragg, and A. Brewer, "Comparative Measurements of Earth and Martian Entry Environments in the NASA Langley HYMETS Facility," AIAA Paper 2011-1014, 49th AIAA Aerospace Sciences Meeting, , January 4-7, 2011, Orlando, FL, 2011.

[13] Cantera High Temperature Air Thermo Library, "airNASA9.cti" accessed from http://code.google.com/p/cantera/source/browse/cantera18/branches/pecos_autotools/data/inputs/airNASA9.cti?r=1493 on February 1, 2014.

[14] Cantera High Temperature Air Thermo Library, "nasa_gas.cti" accessed from http://code.google.com/p/cantera/source/browse/cantera18/trunk/data/inputs/nasa_gas.cti?r=353 on February 1, 2014.

[15] Chemical Equilibrium Calculator, maintained by Colorado State University (using STANJAN solver), accessed from http://navier.engr.colostate.edu/~dandy/code/code-4/ on February 1, 2014.

[16] NASA Chemical Equilibrium with Applications (CEA) Solver, accessed from http://www.grc.nasa.gov/WWW/CEAWeb/ceaHome.htm on February 1, 2014

[17] S.J. Henderson and J.A. Menart, "Equilibrium properties of high-temperature air for a number of pressures," *AIAA Journal of Thermophysics and Heat Transfer*, Vol. 22, No. 4, pp. 718-726, 2008.

[18] Hillensrath, J., and Klein, M., "Tables of Thermodynamic Properties of Air in Chemical Equilibrium Including Second Virial Corrections from 1500 K to 15000 K," Arnold Engineering Development Center TR-65-58, Arnold AFB, TN, 1965."

[19] Y. Cengel and M. Boles, *Thermodynamics: An Engineering Approach, 4*th Ediction, McGraw-Hill, New York, 2001

[20] P. C. Palma, *Laser-Induced Fluorescence Imaging in Free-Piston Shock Tunnels*, PhD Thesis, Australian National University, submitted May 1998, revised February 1999.

[21] J.A. Fulton, J.R. Edwards, H.A. Hassan, R. Rockwell, C. Goyne, J. McDaniel, C. Smith, A. Cutler, C. Johansen, P. Danehy, and T. Kouchi, "Large-Eddy / Reynolds-Averaged Navier-Stokes Simulations of a Dual-Mode Scramjet Combustor," AIAA 2012-0115 50th AIAA Aerospace Sciences Meeting, Jan 9-12, 2012

[22] G. Herzberg, *Molecular Spectra and Molecular Structure: I. Spectra of Diatomic Molecules*, 2nd Ed, Kreiger, Malabar, Florida. 135, 1989.

[23] Eckbreth, Alan C. *Laser diagnostics for combustion temperature and species*, CRC Press, 1996.

[24] W.G. Vincenti and C.H. Kruger, *Introduction to Physical Gas Dynamics*, Wiley & Sons, 1965.

[25] J.D. Anderson, *Hypersonic and High-Temperature Gas Dynamics,* AIAA Educational Series, 2nd Ed., 2006.